2020 IEEE/RSJ International Conference on Intelligent Robots and Systems (IROS)
October 25-29, 2020, Las Vegas, NV, USA (Virtual)

Jumping Motion Generation for Humanoid Robot Using Arm Swing Effectively and Changing in Foot Contact Status *

H. Mineshita, T. Otani, M. Sakaguchi, Y. Kawakami, and H.O. Lim, *Member, IEEE*
and A. Takanishi, *Fellow, IEEE*

Abstract— **Human jumping involves not only lower limbs but also whole-body coordination. During jumping, the effect of sinking the center of mass for recoil and arm swing are significant, and they can cause changes in the jump height. However, upper body movements during jumping movements of humanoid robots have not been studied adequately. When jumping involves only the lower limbs, the burden on the lower limbs increases and it is difficult to jump as high as humans do. Also, if the sole is in contact with the ground during jumping movements, we cannot make good use of the ankle joint. Humans raise their heels during jumping movements, but there are few cases where humanoid robots achieve these movements. Therefore, we thought that jumping with recoil motion by the sinking, arm swing, and changing in foot contact status could result in a higher jump height higher than that possible with only lower limb movements. Hence, in this study, we generated jumping motion using sinking, arm swing and changing foot posture. First, a center of mass trajectory was generated by planning the entire jumping motion, and at the same time, the angular momentum was determined for stability. Next, the joint trajectory was calculated using these two parameters. At that time, arm trajectory and foot posture were specified in the null space. This generated a jumping motion considering arm swing. During simulations, this method provided a jump height almost four times the jump height that obtained without arm swing.**

*Research was supported by the Research Institute for Science and Engineering, Waseda University; Humanoid Robotics Institute, Waseda University; Human Performance Laboratory, Waseda University; Future Robotics Organization, Waseda University. It was also financially supported in part by the JSPS KAKENHI Grant No. 17H00767. Further, 3DCAD software SolidWorks was provided by SolidWorks Japan K.K.; the force sensors were procured from Tec Gihan Co., Ltd.; cables and connectors were provided by DYDEN CORPORATION; the high-performance physical modeling and simulation software MapleSim used in this research was provided by Cybernet Systems Co., Ltd. (Vendor: Waterloo Maple Inc.) We would also like to thank Editage (www.editage.jp) for English language editing services.

Hiroki Mineshita is with the Graduate School of Modern Mechanical Engineering, Waseda University, #41-304, 17 Kikui-cho, Shinjuku-ku, Tokyo 162-0044, Japan (e-mail: contact@takanishi.mech.waseda.ac.jp).

Takuya Otani is with the Research Institute for Science and Engineering, Waseda University, and is a researcher at the Humanoid Robotics Institute (HRI), Waseda University.

Masanori Sakaguchi is with the ASICS Corporation, Institute of Sport Science.

Yasuo Kawakami is with the Faculty of Sport Science, Waseda University.

Hun-ok Lim is with the Faculty of Engineering, Kanagawa University, and is a researcher at the Humanoid Robotics Institute (HRI), Waseda University.

Atsuo Takanishi is with the Department of Modern Mechanical Engineering, Waseda University, and is the director of the Humanoid Robotics Institute (HRI), Waseda University

I. Introduction

In recent years, various types of industrial robots have been introduced with increasing process automation in factories. However, these robots are larger and heavier than humans. The weight of an industrial robot arm capable of lifting 250 kg, lifted by Olympic athletes during weightlifting [1], can reach as high as 1 t. The reason why humans achieve high performance even though they are smaller and lighter than robots is because of whole-body coordination. During weightlifting, the weight is lifted using all the muscles.

Therefore, focusing on whole-body coordination, we considered developing a robot capable of dynamic motions with high efficiency. To confirm this possibility, we examined movements performed during and we selected vertical jumping; this movements actually confirmed to have the ability improvement by weightlifting [2]. Vertical jumping is characterized by recoil motion is performed by sinking [3] and whole-body coordination involving arm swing and trunk movement; human use these movements to increase the jump height [4]. The elasticity of the lower limb joint, especially Achilles tendon, plays an important role [5]. In addition, there are joint asynchronous joint movements in the lower limbs, occurring in the following order: hips, knees, and ankles [6]. Furthermore, transition to the standing on the tiptoe [7].

We focused on whole-body coordination, involving arm swing, trunk movement, and changing in foot posture. There are many studies on humanoid robots performing vertical jumps. For example, Honda's ASIMO is capable of single and double leg continuous jumping [8] and Boston Dynamics' Atlas is capable of double-legged jumping and even dive roll [9]. And they use the sinking of the COM to jump. But few studies focus on arm swing and foot posture. In one study, the joint trajectory of the arm is calculated via optimization to increase the ground reaction force (GRF) during the sinking motion to jumping, and AIST's HRP-2 jumps during the simulation, but the robot did not swing its arm like humans [10]. There is also research on jumping motions focusing on foot posture [11]. In this research, they approximated the robot with a four-link model and optimized the motion of each joint to generate a jumping motion with the standing on the tiptoe. But this is a study on legged robots and does not consider coordination of the upper body. Hence, in this study, we generate the trajectory of the arm and foot posture and generated a jumping motion with the sinking motion and whole-body coordination considering these trajectories.

978-1-7281-6211-9/20/$31.00 ©2020 IEEE

II. Motion Generation and Whole-Body Coordination During Jumping

A. Concept of Motion Generation

We determined the method for generating jumping motion. The center of mass (COM) trajectory is the main parameter considered when planning whole-body motion. Jump height can be defined as the height of the COM or the distance between the foot and ground. When analyzing the dynamics of jumping, we can analyze the energy. To do so, we determined the height of the COM, which is a measure of the potential energy. Therefore, we decided to focus on the height of the COM rather than the distance between the foot and ground.

Therefore, we decided to generate the COM trajectory using the loaded inverted pendulum model when generating whole-body motion. The conservation of momentum holds while in the air, and the attitude of the robot is determined by its rotation around the COM and angular momentum at the moment of the jump. Therefore, we decided to determine the angular momentum for ensuring stability in the air. Furthermore, the condition that the toe should not move was set to consider contact with the ground during the jumping motion. The joint trajectory during jumping motion can be generated by calculating from the two conditions of this angular momentum and toe speed in the same way [12] as for the center of gravity (COG) Jacobian [13].

However, this method does not generate a large arm swing like that generated by a human. In addition, the jumping motion starts from a state where the toe and heel are in contact with the ground, thus ensuring a stable starting posture. Unless the position of the heel is specified, the only condition is that the toe does not move, so that an action that causes the heel to sink into the ground may be generated. In addition, raising the heel during the jumping motion enables the use of the lower limb joint, especially the ankle joint. Therefore, it is necessary to restrain foot movement to some extent. Hence, we decided to calculate the arm joint trajectory is in advance and calculate the foot posture trajectory when necessary; the whole-body joint trajectory for realizing these trajectories could be generated by adding these trajectories to the null space.

B. COM Trajectory Generation

We decided to use a spring loaded inverted pendulum (SLIP; [14]) model with linear motion as the vertical model for generating the COM trajectory. The calculation was performed using the single-mass model presented in Fig. 1(a). The equation of motion for this model is as follows:

$$m\ddot{l} - kz = 0, \tag{1}$$

where, m is the mass of mass M, l is the position of the linear part, k is the elastic modulus of the leg spring, and z is the length till where from the natural length of the leg spring. In this model, a sine wave that causes forced oscillation in the spring part is generated in the linear motion part. In this case, because the arm is considered separately, the model resembles that shown in Fig. 1(b), and the equation at this time is as follows:

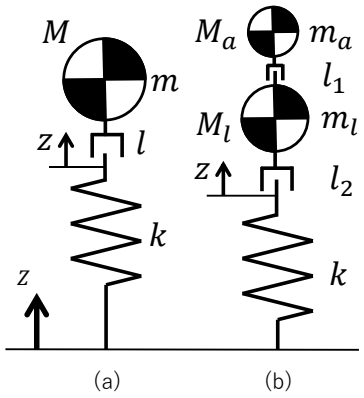

Fig. 1 SLIP model with linear motion.

$$m_a\ddot{l}_1 + (m_a + m_l)\ddot{l}_2 - kz = 0, \tag{2}$$

where, m_a is the mass of mass M_a corresponding to the arm, m_l is the mass of mass M_l corresponding to the part other than the arm, and l_1 and l_2 are the z-axis positions of the upper and lower linear motion parts, respectively. In Fig. 1(a), the trajectory of l is calculated as a sine wave that causes forced oscillation in a spring, and the mass trajectory at that time is set as the target COM trajectory. In this study, to calculate the trajectory of the arm in advance, l_1 and l_2 in Eq. (2) were calculated considering the movement of the arm. From this equation, the sinking motion for recoil is generated.

Next, we considered the forward and backward, motions along the x-axis. The projection point of the COM on the ground must be within the supporting polygon formed by the toe and heel during the initial posture. However, at the moment of jumping, the COM needs to be directly above the toe because the posture transitions to standing on the tiptoe. Therefore, we planned to move the COM to the toe before transitioning to standing on the tiptoe. The x-axis motion was calculated using a quintic equation so that the initial and terminal velocities and accelerations were zero. At this time, stability was not considered; however, if the trajectory become unstable, it was corrected using the angular momentum trajectory.

C. Angular Momentum Trajectory Generation

The zero moment point (ZMP) must be at the tiptoe while standing on the tiptoe. Therefore, the angular momentum was set so that the ZMP was always at the tiptoe. The ZMP can be calculated using the moment which act on the floor [15]. The angular momentum can be calculated by integrating this moment. Therefore, we utilized it in the formula to find the ZMP as follows:

$$\begin{cases} \dot{L}_x = (mg + \dot{P}_z)Z_y - mgC_y - Z_z\dot{P}_y \\ \dot{L}_y = -(mg + \dot{P}_z)Z_y + mgC_x + Z_z\dot{P}_x \\ \dot{L}_z = 0 \end{cases}, \tag{3}$$

where, $\boldsymbol{L} = [L_x \quad L_y \quad L_z]^T$ is the angular momentum; $\boldsymbol{P} = [P_x \quad P_y \quad P_z]^T$ is the translational momentum; $\boldsymbol{Z} = [Z_x \quad Z_y \quad Z_z]^T$ is the ZMP position;

$\boldsymbol{C} = [C_x \quad C_y \quad C_z]^T$ is the COM position; g is the gravitational acceleration; m is the total mass, all of which were calculated in the world coordinate system. When standing on the tiptoe, the moment was calculated using Eq. (3); this moment was then integrated to calculate the angular momentum. Motions during other periods were generated using quintic equations. As the robot does not move in the initial posture, the initial value was considered the angular momentum and its first and second derivatives were set to zero, and the end value was calculated using Eq. (3). ZMP is calculated with a margin, but it is verified after motion generation and ZMP is redesigned if it falls.

D. Arm Joint Trajectory Generation

Next, we generated the arm joint trajectory. The upward and downward swinging motions were generated by specifying three parameters, namely the initial posture, the lowest point of the swing, and the top point of the swing. These were calculated using the fifth order spline between each target value. At this time, the speed and acceleration at each time were set to zero. The axes specified here are the pitch axes of the shoulder and elbow. In future, it is possible to use the actual human arm swing as the trajectory and generate it from the desired COM trajectory of the arm.

E. Foot Posture Trajectory Generation

The foot posture is specified by the following conditions. First, the heel is not raised while the sole touches the ground, that is, the foot posture is maintained parallel to the ground. During this time, the foot posture speed is zero. Next, when the angle of the lower limb joint, especially the ankle joint, is about to exceed the limit of the movable angle, the foot posture is controlled to keep it within the movable range. It is on the dorsiflexion side that the ankle joint is likely to reach the limit angle, and raising the heel can avoid it. Therefore, a point near the limit value within the movable angle range was set as the threshold, and the posture that raised the heel by the excess of joint angle from threshold was set as the target foot posture. Finally, if the heel became lower than toe, that is, if the heel is likely to sink into the ground, the foot was kept parallel to the ground so that the heel did not sink into the ground. In this case, the angle between the foot and ground was set as the target. In other cases, the foot posture was not controlled to reduce lower limb joint constraint. The foot posture can be calculated from the base link posture and leg joint angles. These were calculated as needed. Our main objective was to maintain sole contact, consider the limit of the movable angle, and prevent the heel from sinking into the ground. We assumed that the movable angle limit was not reached during sole contact.

F. Whole-Body Joint Trajectory Generation

Using the trajectories calculated in B to E, the whole-body joint trajectory was generated. In this study, we used the concept of the COG Jacobian. First, we developed the following equations:

$$\boldsymbol{A}_p\dot{\boldsymbol{p}}_0 + \boldsymbol{A}_\omega\boldsymbol{\omega}_0 + \boldsymbol{A}_\theta\dot{\boldsymbol{\theta}} = \tilde{\boldsymbol{L}}, \tag{4}$$

$$\dot{\boldsymbol{p}}_{F1} = \dot{\boldsymbol{p}}_0 + \boldsymbol{\omega}_0 \times \boldsymbol{R}_0\,{}^0\boldsymbol{p}_{F1} + \boldsymbol{R}_0\,{}^0\boldsymbol{J}_{F1}\dot{\boldsymbol{\theta}}, \tag{5}$$

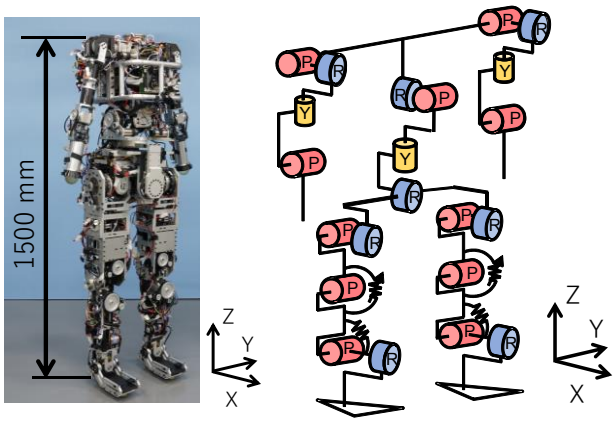

(a) Robot (b) DOF Configuration

Fig. 2. WATHLETE-1. The robot has 22 DOF. Blue, red, and yellow joints denote the roll, pitch, and yaw axes, respectively, in (b).

where, $\boldsymbol{A}_p\dot{\boldsymbol{p}}_0$ is the term representing the base link translation velocity in the angular momentum; $\boldsymbol{A}_\omega\boldsymbol{\omega}_0$ is the term indicating the base link angular velocity in the angular momentum; $\boldsymbol{A}_\theta\dot{\boldsymbol{\theta}}$ is the term denoting the joint angular velocity in the angular momentum; $\tilde{\boldsymbol{L}}$ is the target angular momentum; $\boldsymbol{p}_{F1}$ is the position of the toe (F1) ; $\boldsymbol{p}_0$ is the base link position; $\boldsymbol{\omega}_0$ is the base link angular velocity; $\boldsymbol{R}_0$ is the rotation matrix from world coordinates to base link coordinates; ${}^0\boldsymbol{p}_{F1}$ is the position of the toe in base link coordinates; ${}^0\boldsymbol{J}_{F1}$ is the Jacobian that connects the toe and the joint speeds; $\dot{\boldsymbol{\theta}}$ is the joint speed. The joints generated by this method are symmetrical patterns with the pitch axes of the shoulder, elbow, trunk, hip, knee, and ankle joint. Therefore, $\boldsymbol{\theta}$ is a six-dimensional vector. If Eqs. (4) and (5) are combined considering the movement of the base link, these equations can be transformed as follows:

$$\begin{bmatrix}\dot{\boldsymbol{p}}_0 \\ \boldsymbol{\omega}_0\end{bmatrix} = \boldsymbol{J}'\dot{\boldsymbol{\theta}} + \boldsymbol{V}'\begin{bmatrix}\dot{\boldsymbol{p}}_{F1} \\ \tilde{\boldsymbol{L}}\end{bmatrix}, \tag{6}$$

where, $\boldsymbol{J}'$ is the Jacobian that connects the movement of the base link and joint speeds; $\boldsymbol{V}'$ is the coefficient of the target value of foot posture speed ($\dot{\boldsymbol{p}}_{F1}$) and angular momentum ($\tilde{\boldsymbol{L}}$). The motion of the base link and the motion of the COM are expressed as follows:

$$\dot{\boldsymbol{p}}_0 + \boldsymbol{\omega}_0 \times \boldsymbol{R}_0\,{}^0\boldsymbol{p}_G + \boldsymbol{R}_0\,{}^0\boldsymbol{J}_G\dot{\boldsymbol{\theta}} = \dot{\boldsymbol{p}}_G, \tag{7}$$

where, ${}^0\boldsymbol{p}_G$ is the position of the COM in base link coordinates; ${}^0\boldsymbol{J}_G$ is the Jacobian connecting the COM and joint speeds in the base link coordinates; $\boldsymbol{p}_G$ is the position of the COM in world coordinates. Substituting Eq. (7) into Eq. (6) yielded the following equation:

$$\dot{\boldsymbol{\theta}} = \boldsymbol{J}_G{}^+\left(\dot{\boldsymbol{p}}_G - \boldsymbol{V}\begin{bmatrix}\dot{\boldsymbol{p}}_{F1} \\ \tilde{\boldsymbol{L}}\end{bmatrix}\right) + (\boldsymbol{I} - \boldsymbol{J}_G{}^+\boldsymbol{J}_G)\boldsymbol{k}, \tag{8}$$

where, $\boldsymbol{J}_G$ is the Jacobian connecting the joint velocities and COM velocities; $\boldsymbol{V}$ is the coefficient the target value of foot

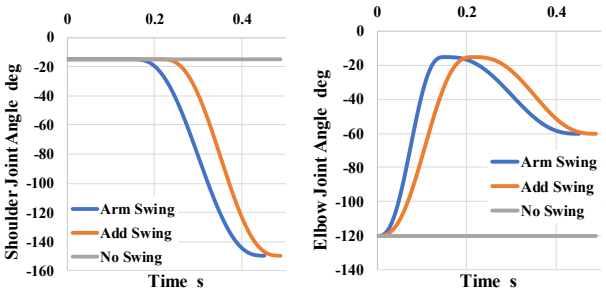

(a) Shoulder (b) Elbow

Fig. 3. Comparison of arm joint trajectories of each motion.

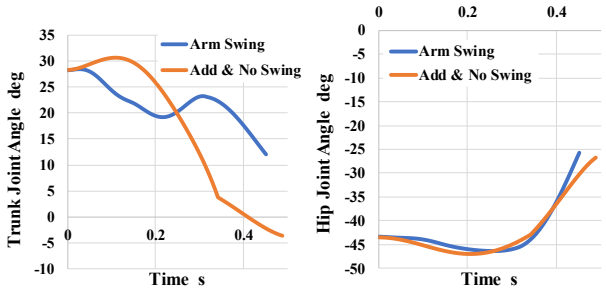

(a) Trunk (b) Hip

Fig. 4. Comparison of trunk and hip joint trajectories of each motion.

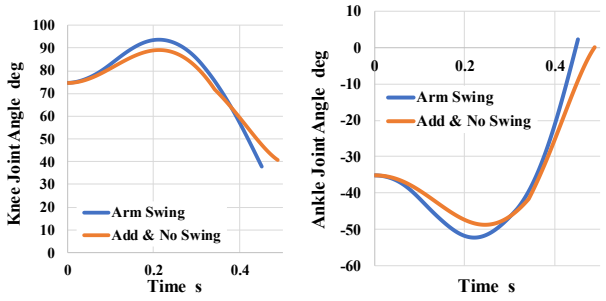

(a) Knee (b)Ankle

Fig. 5. Comparison of knee and ankle trajectories of each motion.

posture speed ($\dot{\boldsymbol{p}}_{F1}$) and angular momentum ($\tilde{\boldsymbol{L}}$); $\boldsymbol{I}$ is the identity matrix; $\boldsymbol{k}$ is any vector. $\tilde{\boldsymbol{L}}$ was planned in C, and $\dot{\boldsymbol{p}}_{F1}$ is always $[0 \quad 0 \quad 0]^T$ because the toe does not move while touching the ground. The second term of Eq. (8) indicates that there is redundancy; thus, by properly setting $\boldsymbol{k}$, the condition can be added to the null space [16]. To apply the values mentioned in D and E in the null space, a Jacobian was generated and connected to $\dot{\boldsymbol{\theta}}$, respectively as follows:

$$\dot{\boldsymbol{\theta}} = \boldsymbol{J}_{arm}\dot{\boldsymbol{\theta}}_{arm}, \tag{9}$$

$$\dot{\boldsymbol{\theta}} = \boldsymbol{J}_{F\omega}\boldsymbol{\omega}_F, \tag{10}$$

where, $\dot{\boldsymbol{\theta}}_{arm}$ is the arm joints trajectory described in D; $\boldsymbol{\omega}_F$ is the foot posture trajectory explained in E. In this time, $\dot{\boldsymbol{\theta}}_{arm}$ is a two-dimensional vector to indicate the pitch axis of the shoulder and elbow, and $\boldsymbol{\omega}_F$ is a one-dimensional vector to specify only the posture around the pitch axis. $\boldsymbol{k}$ was appropriately fixed using these Eqs. (9) and (10) and used for joint trajectory generation in the null space.

TABLE I. RESULTS OF SIMULATION

Motion type		No Swing	Add Swing	Arm Swing
Coordinated joints	-	Only the leg and the trunk		Whole body
Arm swing	-	No	Yes	
Max power in the leg	W	400	400	400
Max power in the arm	W	0	500	350
Flight duration	ms	90	70	220
Jumping height	mm	22	13	80

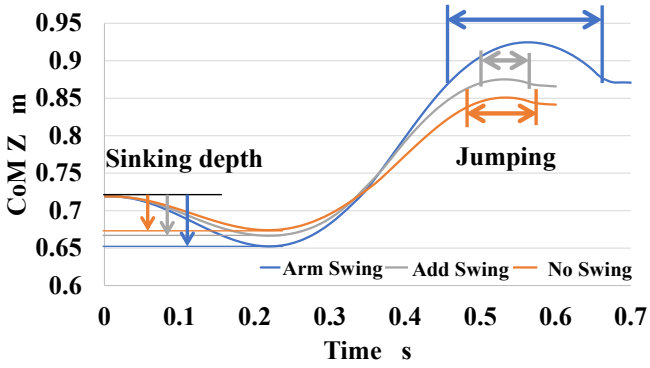

Fig. 6. Comparison of COM trajectories in the simulation.

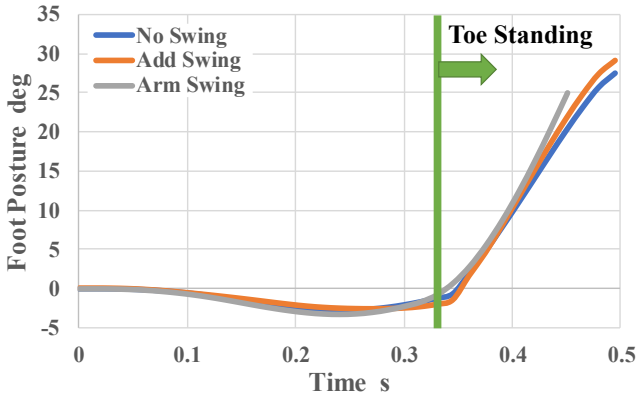

Fig. 7. Comparison in foot posture trajectories in the simulation.

TABLE II. MAXIMUM INSTANTANEOUS OUTPUT OF EACH JOINT

Joint Output		No Swing	Add Swing	Arm Swing
Shoulder	W	-	500	350
Elbow	W	-	80	200
Trunk	W	80	420	100
Hip	W	120	200	150
Knee	W	400	400	400
Ankle	W	300	250	300

III. SIMULATIONS

The effectiveness of the proposed method was verified through simulations. The simulation was performed using the model of our biped humanoid robot WATHLETE-1 (Waseda ATHLETE humanoid No. 1; Fig. 2). This robot has the same link length and weight as that of humans, 22 degree of freedom (DOF), and elastic elements at the knee and ankle joint [12]. In addition, upper body simulates the moment of inertia that of humans [17]. In the simulation environment, no elastic elements were mounted on the joint. To confirm the effectiveness of our method, we compared motion in the following three scenarios during the simulation; motion without swinging the arms (No Swing), motion generated in No Swing with arm joint trajectory (Add Swing), and motion

generated using the proposed method, where the arm swing is given by null space (Arm Swing). Each movement was adjusted so that the maximum instantaneous output of the knee, which is the maximum output power in the leg, was approximately 400 W. Also, standing on the tiptoe is set for the last 30% of the jumping motion. In this case, the heel lift due to the limit of the movable angle was not generated. Furthermore, the spring property of the legs in Fig. 1(a) model was set to 5600 N/m. This was calculated from the COM trajectory of the human jump measured in the previous study [18]. In No Swing, the pitch axes of the shoulder and elbow were fixed in the initial posture.

The joint motion at this time is shown in Fig. 3, Fig. 4, and Fig. 5, and the simulation results are presented in TABLE I, TABLE II, Fig. 6, and Fig. 7. Fig. 8 shows frame-by-frame images of the simulation. According to these simulation results, the proposed method (Arm Swing) increased almost four times the jump height that of No Swing. This could be because the load on the leg was successfully reduced through recoiling of the arm. Compared to the COM trajectory, Arm Swing involved a deeper recoil (sinking) than Add Swing or No Swing. Deeper sinking resulted in higher force on the lower limb joints, but the maximum instantaneous output at the knee was the same in the three scenarios. These loads were the outputs from the shoulders and elbows. However, in Add Swing, the jump height was lower than that in No Swing because the recoil of the arm hindered the jumping motion. This shows that the proposed method is effective for whole-body coordination, especially arm swing, and improves the jump height.

Looking at the foot posture, as planned, 30% behind the jumping motion is transitioning to standing on the tiptoe (See Fig. 7). Since the stability is maintained during standing on the tiptoe, the stabilization by this method has been successful. Before shifting to standing on the tiptoe, the foot posture is slightly reversed (so that the toe floats). This caused by the effect of the elasticity in the grounding point (rubber hemisphere) mounted on toe and heel. This is because the ZMP approaches the heel by the forward movement of the COM, and a large GRF is generated at the heel (See Fig. 8).

Next, when comparing the joint trajectories (See Fig. 4, Fig. 5, and Fig. 6), there are differences in all joints especially in trunk, knee, and ankle joints. The reason why the shoulder and elbow trajectories are different between Arm Swing and Add Swing is that the pattern time is longer in Add Swing. For the knee and ankle joints, the rotation angle in Arm Swing is larger than No Swing. This is thought to have been generated to achieve a deeper sinking. Because the COM is located near

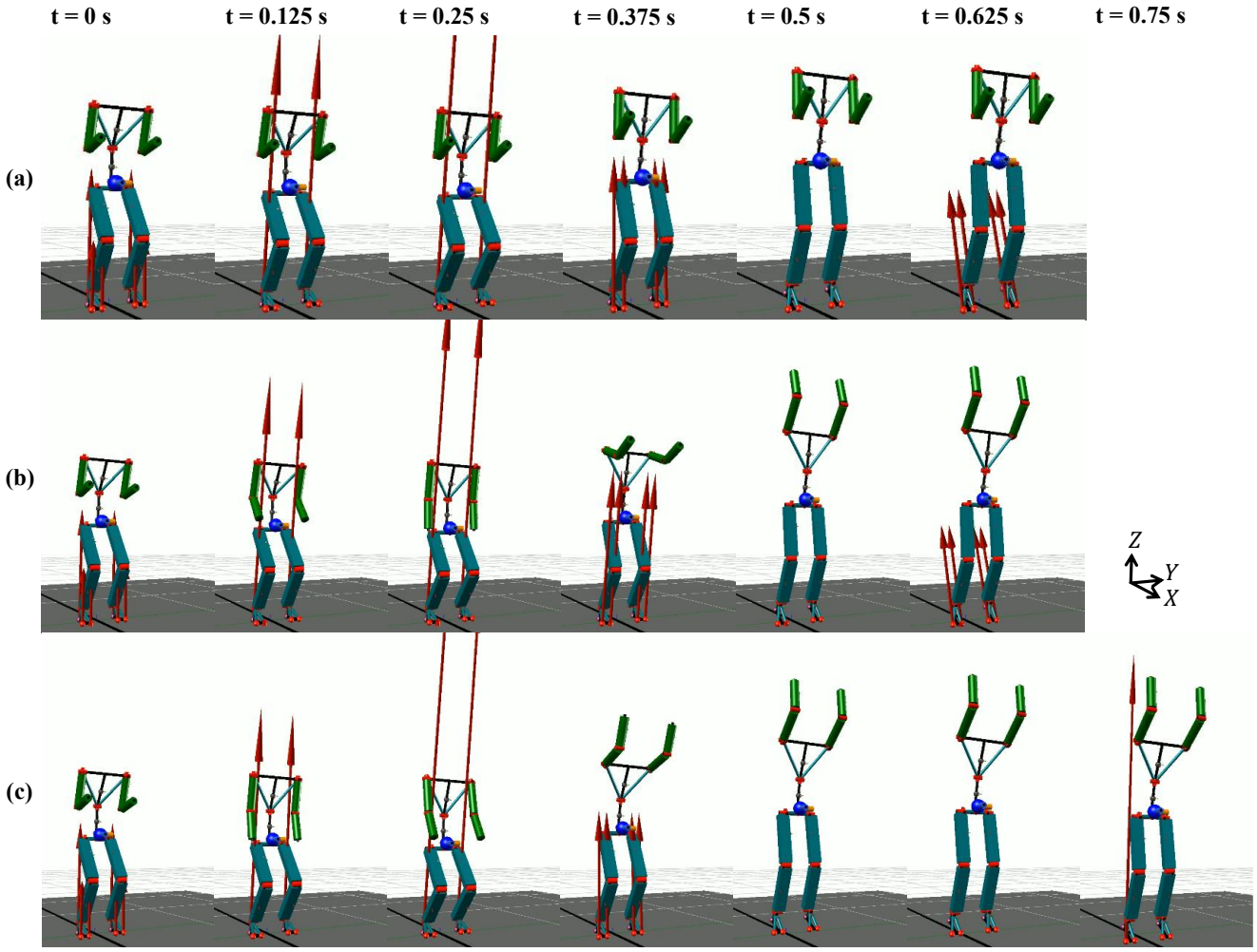

Fig. 8. Frame-by-frame images of simulation. (a), (b), and (c) is the No Swing, Add Swing, and Arm Swing motion, respectively. The red arrows in the images indicate the ground reaction force at each contact point.

the pelvis, the lower limb joints, especially the knee and ankle joints, are considered to be greatly affected. On the other hand, the trajectory of the trunk differs greatly between Arm Swing and No Swing. This is considered to suppress the recoil of the movement of the arm. The arm swings quickly and greatly, which increases the moment of inertia and the displacement of the COM trajectory. It is considered that the large motion difference occurred in trunk because it was closed to the arm. On the other hand, there was little difference in the hip joint. Because of using Jacobian in this method, the motion that minimizes the angular velocities of the joints were selected by minimizing the norm. It is considered that the rotation of the hip joint, which is less affected by the movement of the COM and the rotation of the arm, was reduced. In the case of a human jump, hip and trunk are greatly bent in order to greatly depress the upper body posture, but in this operation, the posture is mainly depressed only by the trunk. When comparing the output with Arm Swing, the descending order is as follows: knees, shoulders, ankles, elbows, hips, and trunks (See TABLE II). The output trends are similar for Arm Swing and No Swing, but Add Swing is very different. This is probably because the coordination of the whole-body was disrupted by simply adding arm trajectory, and the load on the joints increased. When comparing the output between No Swing and Arm Swing, there is almost no difference in the total of the legs and trunk, but output is large in the arm at Arm Swing. This shows that the arm has a significant effect on the height of the jump. In the future, we will study the adaptation of the weight matrix so that the load can be shared according to the output of each joints and the leaf springs mounted on the knee and ankle joints can be used effectively.

Moreover, the simulation results are within the output range of WATHLETE-1 and can be sufficiently reproduced using a real robot. We will proceed with experiments using an actual robot.

IV. CONCLUSION AND FUTURE WORKS

In this study, we tried to improve the jump height of a robot by effectively using the arm swing motion and changing foot posture. Involved jump heights could be achieved using this jumping method, without increasing the load on the leg joint. We validated our method through simulations, the jump achieved using our method was almost four times the jump height that obtained with no arm swing.

However, the operation this method only generates the motion in the x-z plane, and the operation in the y axis direction has not been considered. In the simulation, there was no problem in the model because the robot, WATHLETE-1, was symmetric with respect to the x-z plane. However, it is considered that there are model errors due to wiring etc. For this, it is necessary to control the GRF, ZMP, etc. and correct the COM trajectory, but it is difficult to control by the proposed method because the calculation cost is heavy. For this reason, in control, it is conceivable to develop methods with lower calculation cost, or to reduce the calculation cost by performing some calculations in advance.

Also, in this method, although the motion can be output using the actual robot, a large output is required for the arm that cannot exert strong force that of humans. Therefore, it is necessary to reduce arm joints outputs by introduction of weight matrix according to the differences of each joints output and the optimization for joint output in the future.

In addition, we will aim to conduct experiments using the actual robot, because this method was only evaluated on the simulation.

REFERENCES

[1] "Rio 2016/Weightlifting Videos - Best Olympic Videos," *International Olympic Committee*, Jan. 14, 2018. https://www.olympic.org/videos/rio-2016/weightlifting (accessed Jul. 20, 2020).

[2] D. Hackett, T. Davies, N. Soomro, and M. Halaki, "Olympic weightlifting training improves vertical jump height in sportspeople: a systematic review with meta-analysis," *Br. J. Sports Med.*, vol. 50, no. 14, pp. 865–872, Jul. 2016, doi: 10.1136/bjsports-2015-094951.

[3] K. Mackala, J. Stodólka, A. Siemienski, and M. Coh, "Biomechanical Analysis of Squat Jump and Countermovement Jump From Varying Starting Positions," *J. Strength Cond. Res.*, vol. 27, no. 10, pp. 2650–2661, Oct. 2013, doi: 10.1519/JSC.0b013e31828909ec.

[4] E. A. Harman, M. T. Rosenstein, P. N. Frykman, and R. M. Rosenstein, "The effects of arms and countermovement on vertical jumping," *Med. Sci. Sports Exerc.*, vol. 22, no. 6, p. 825, Dec. 1990.

[5] N. Sugisaki, J. Okada, H. Kanehisa, and T. Fukunaga, "Effect of elastic energy on the mechanical work and power enhancement in counter movement exercise of ankle joint," *Jpn. J. Ergon.*, vol. 40, no. 2, pp. 82–89, 2004, doi: 10.5100/jje.40.82.

[6] G. J. Van Ingen Schenau, "From rotation to translation: Constraints on multi-joint movements and the unique action of bi-articular muscles," *Hum. Mov. Sci.*, vol. 8, no. 4, pp. 301–337, Aug. 1989, doi: 10.1016/0167-9457(89)90037-7.

[7] M. F. Bobbert and G. J. van Ingen Schenau, "Coordination in vertical jumping," *J. Biomech.*, vol. 21, no. 3, pp. 249–262, Jan. 1988, doi: 10.1016/0021-9290(88)90175-3.

[8] "Honda Global | ASIMO." https://global.honda/innovation/robotics/ASIMO.html#2011 (accessed Feb. 11, 2020).

[9] "Atlas® | Boston Dynamics." https://www.bostondynamics.com/atlas (accessed Jul. 20, 2020).

[10] S. Sakka and K. Yokoi, "Humanoid Vertical Jumping based on Force Feedback and Inertial Forces Optimization," in *Proceedings of the 2005 IEEE International Conference on Robotics and Automation*, Apr. 2005, pp. 3752–3757, doi: 10.1109/ROBOT.2005.1570692.

[11] X. Wan, T. Urakubo, and Y. Tada, "Optimization of jumping motion of a legged robot for different take-off postures," *J. Mech. Sci. Technol.*, vol. 29, no. 4, pp. 1391–1397, Apr. 2015, doi: 10.1007/s12206-015-0309-5.

[12] T. Otani *et al.*, "Jumping Motion Generation of a Humanoid Robot Utilizing Human-Like Joint Elasticity," in *2018 IEEE/RSJ International Conference on Intelligent Robots and Systems (IROS)*, Oct. 2018, pp. 8707–8714, doi: 10.1109/IROS.2018.8594085.

[13] T. Sugihara and Y. Nakamura, "Whole-body Cooperative Reaction Force Manipulation on Legged Robots with COG Jacobian involving Implicit Representation of Unactuated Coordinates," *J. Robot. Soc. Jpn.*, vol. 24, no. 2, pp. 222–231, Mar. 2006, doi: 10.7210/jrsj.24.222.

[14] Raibert M. H., *Legged robots that balance*. MIT Press, 1986.

[15] A. Takanishi, M. Ishida, Y. Yamazaki, and I. Kato, "The Realization of Dynamic Walking by the Biped Walking Robot WL-10 RD," *J. Robot. Soc. Jpn.*, vol. 3, no. 4, pp. 325–336, 1985, doi: 10.7210/jrsj.3.325.

[16] H. Hanafusa, T. Yoshikawa, and Y. Nakamura, "Redundancy Analysis of Articulated Robot Arms and Its Utilization for Tasks with Priority," *Trans. Soc. Instrum. Control Eng.*, vol. 19, no. 5, pp. 421–426, 1983, doi: 10.9746/sicetr1965.19.421.

[17] T. Otani *et al.*, "Upper-Body Control and Mechanism of Humanoids to Compensate for Angular Momentum in the Yaw Direction Based on Human Running," *Appl. Sci.*, vol. 8, no. 1, p. 44, Jan. 2018, doi: 10.3390/app8010044.

[18] A. Lees, J. Vanrenterghem, and D. D. Clercq, "Understanding how an arm swing enhances performance in the vertical jump," *J. Biomech.*, vol. 37, no. 12, pp. 1929–1940, Dec. 2004, doi: 10.1016/j.jbiomech.2004.02.021.